

# Quasi-harmonic vs. “exact” surface free energies of Al: a systematic study employing a new interatomic potential

U. Hansen,<sup>1</sup> P. Vogl,<sup>1</sup> and Vincenzo Fiorentini<sup>1,2</sup>

1) *Physik-Department and Walter Schottky Institut, Technische Universität München, D-85748 Garching, Germany*

2) *Istituto Nazionale per la Fisica della Materia and Dipartimento di Fisica, Università di Cagliari, Italy*  
(to appear on PRB)

We discuss a computationally efficient classical many-body potential designed to model the Al-Al interaction in a wide range of bonding geometries. We show that the potential yields results in properties in excellent agreement with experiment and *ab initio* results for a number of bulk and surface properties, among others for surface and step formation energies, and self-diffusion barriers. As an application, free energy calculations are performed for the Al (100) surface by Monte Carlo thermodynamic integration and the quasi-harmonic approximation. Comparison of the latter approximation with the reference Monte Carlo results provides informations on its range of applicability to surface problems at high temperatures.

PACS: 05.70.Ce 05.10.Ln 05.70.Np 82.20.Kh

## I. INTRODUCTION

Atomistic simulations are playing an increasingly prominent role in materials science. From studies of crystallization of clusters<sup>1</sup> to large-scale simulations of fracture<sup>2</sup> and grain boundary diffusion<sup>3</sup>, atomistic simulations offer a microscopic physical view that cannot be obtained from experiment. Predictions resulting from this atomic level understanding are proving increasingly accurate and useful.<sup>4</sup>

The effective interatomic interaction potential is the key ingredient in all atomistic simulation. The accuracy of the potential affects drastically the quality of the simulation result, and its functional complexity determines the amount of computer time required.<sup>5</sup> Much research effort has therefore been devoted to the design of potential energy functions.<sup>6</sup> This is especially important in classical dynamics which, although quantum mechanical simulations have been progressing at a rapid pace in recent years, remains the most (sometimes, the only) affordable way to perform very large scale simulations in materials science. In this paper, we present a new carefully designed Al-Al interaction model, test its performance, and we apply it to the study of free energies in atomic scale simulations.

The ability to compute free energies is essential to understand or predict many physical phenomena, from the stability of crystal structures, to the propensity to form defects or disorder, and to morphology changes and phase transitions. However, the determination of free energies from atomic scale computer simulations is a daunting task. Approximate methods, mostly based on the harmonic vibrational properties of the system, are commonly in use to this end. Here, we compare several possible versions of the so called quasi-harmonic approximation, using as reference accurate simulation using canonical or constant-pressure Monte Carlo methods and thermodynamic integration, focusing on the specific case of surface

free energies. The goal is to provide a measure of the range of applicability of approximate methods for complex systems using a reliable Al interaction model.

## II. AL INTERACTION POTENTIAL

Previously developed interatomic potentials<sup>7–10</sup> for the Al-Al interaction have mostly focused on bulk and molecular properties. In this work, we analyze and generalize one of those models with special regard to surface properties, aiming as usual at describing Al in as wide a range of chemical environments as possible, *i.e.* ranging from bulk Al to Al surfaces and surface steps, and to small Al molecules. The functionalities of the refined potential are found to extend significantly those of previous ones. As we are going to use an embedded atom interaction model, in this Section we briefly review the basic ideas of this approach, describe the details of the model, and finally assess its quality.

### A. Theory

In the embedded atom method, each atom in a solid is viewed as an impurity embedded in a host comprising all the other atoms.<sup>11,12</sup> The energy of the host with impurity is, according to Stott and Zaremba,<sup>13</sup> a functional of the unperturbed host electron density, and a function of the impurity type and position,

$$E = \mathcal{F}_{Z,R}[\rho_h(\mathbf{r})], \quad (1)$$

where  $\rho_h(\mathbf{r})$  is the unperturbed host electron density, and  $Z$  and  $R$  are the type and position of the impurity. Here the energy of an impurity is determined by the electron density of the host before the impurity is added. The functional  $\mathcal{F}$  is a universal function, independent of the host, but its form is unknown.<sup>11</sup> A simple approximation

to  $\mathcal{F}$  is the so called local approximation, whereby the impurity experiences a locally uniform electron density.<sup>12</sup> This can be viewed as the lowest-order term of an expansion involving the successive gradients of the density. The functional  $\mathcal{F}$  is then approximated by

$$E = F_i(\rho_i(R_i)) + \frac{1}{2} \sum_j \phi_{ij}(R_{ij}), \quad (2)$$

where  $\phi_{ij}$  is a pair potential representing the electrostatic interaction,  $R_{ij}$  is the distance between atoms  $i$  and  $j$ , and  $F_i$  denotes the embedding energy. The total energy of the system is a sum over all individual contributions:

$$E_{\text{tot}} = \sum_i F_i(\rho_{h,i}) + \frac{1}{2} \sum_{\substack{i,j \\ i \neq j}} \phi_{ij}(R_{ij}). \quad (3)$$

A further simplification is introduced assuming that the host density  $\rho_{h,i}$  at atom  $i$  is closely approximated by a sum of the atomic densities  $\rho_j$  of the constituent atoms, *i.e.*  $\rho_{h,i} = \sum_{j,(j \neq i)} \rho_j(R_{ij})$ , with  $\rho_j$  being the contribution to the density at atom  $i$  from atom  $j$ . Equation (3) is the form commonly used for molecular dynamics simulations of metals, and is known as embedded atom potential.

## B. Details of the Al-Al interaction potential

The Ercolessi-Adams interaction model for Al was constructed with the so called force matching method<sup>14</sup> and, in contrast to most other empirical models, it gives excellent structural and elastic properties for the bulk along with the correct surface interlayer relaxations at low-index surfaces. Furthermore, we found that the diffusion barriers for surface adatoms obtained by the Ercolessi-Adams model are in fair agreement with *ab initio* calculations,<sup>15–17</sup> whereas those predicted by most other embedded atom potentials differ drastically<sup>18</sup> from *ab initio* results. We therefore started off from the Ercolessi-Adams potential to build our own refined Al-Al interaction. Without affecting the elastic properties and the surface relaxation properties, we introduced the following modifications to the model:

1. An additional term was introduced in the pair potential  $\phi_{ij}$  in order to account for an exponential Born-Mayer-like repulsion at short Al-Al separation.<sup>19</sup> This is a key requirement for studies of *e.g.* physical vapor deposition processes, where the energy of each single atom easily exceeds the thermal energy by as much as three orders of magnitude.
2. In the low density region, three parameters of the embedding function  $F$  were changed in order to improve several reference quantities, namely the Al<sub>2</sub> binding energy, and vibrational frequency, and the

adatom diffusion barrier height on the Al(111) surface (*i.e.* the energy difference between the surface binding site and the saddle point).

3. A fifth-order polynomial cut-off function was introduced, smoothly bringing the potential to zero at an interatomic distance of 5.56 Å (slightly larger than the third-nearest neighbor distance in bulk Al).

The total energy  $E_{\text{tot}}$  of a system containing Al atoms in an arbitrary arrangement is written (see Sec.II A ) as

$$E_{\text{tot}} = \sum_i F(\rho_i) + \frac{1}{2} \sum_{\substack{i,j \\ i \neq j}} \bar{\phi}_{ij}(r_{ij}). \quad (4)$$

The atomic density  $\rho_i$  in arbitrary units is given as

$$\rho_i = \sum_{j,(j \neq i)} \rho(r_{ij}) \times f_c(r_{ij}, R_0, D_0). \quad (5)$$

The sum runs over all atoms that lie within the potential range  $R_0 + D_0$  (5.56 Å), which is enforced by the cutoff function  $f_c(r, R, D)$ . This function is zero for  $r$  exceeding  $R + D$  and unity for  $r$  less than  $R - D$ . For  $r$  within the interval  $(R - D, R + D)$  it is defined according to

$$f_c(r, R, D) = -3 \left[ \frac{r - R}{D} + 1 \right]^5 + \frac{15}{2} \left[ \frac{r - R}{D} + 1 \right]^4 - 5 \left[ \frac{r - R}{D} + 1 \right]^3 + 1. \quad (6)$$

The function  $\rho(r)$  in Eq.(4) is spline-interpolated using the values reported in Table I; the parameters  $R_0$  and  $D_0$  are given in Table II. The embedding function  $F(\rho)$  is also spline-interpolated, and the corresponding values for  $F(\rho)$  are collected in Table III.

The pair potential term in Eq.(4) is written according to

$$\bar{\phi}_{ij} = \left[ \phi(r_{ij}) + (A \exp\{-\lambda r_{ij}\} \times f_c(r_{ij}, R_\phi, D_\phi) - B) \right] \times f_c(r_{ij}, R_0, D_0). \quad (7)$$

The function  $\phi$  is tabulated in Table IV. The first cut-off  $f_c(r_{ij}, R_\phi, D_\phi)$  switches on the exponential repulsive term at small distances ( $r < 2.25$  Å), while  $f_c(r_{ij}, R_0, D_0)$  terminates the interaction range of the potential. The corresponding parameters are given in Table II. The exponential term ensures that one gets a Born-Mayer repulsion at short separations for, *e.g.*, diatomic molecules.<sup>19</sup>

## C. Assessment of the potential

We now present evidence that the potential just described yields satisfactory results for a variety of properties of Al in different environments. In particular we address the bulk, the dimer, low-index surfaces and steps thereon, and self-diffusion on different low-index surfaces;

also included in this test section is the energy dependent sticking coefficient of high energy Al atoms on Al (111). The changes to the potential significantly improved agreement with experiment and other theoretical predictions in several instances where errors were typically of order 50%.

### 1. Bulk properties

By construction our model does not alter the equilibrium lattice constant  $a_0$ , the cohesive energy  $E_{\text{coh}}$  and the elastic properties of the previous model of Ercolessi. We obtain as in Ref. 14  $a_0 = 4.03 \text{ \AA}$ ,  $E_{\text{coh}} = 3.36 \text{ eV}$ ,  $C_{11} = 118 \text{ GPa}$ ,  $C_{12} = 62 \text{ GPa}$  and  $C_{44} = 36 \text{ GPa}$ . For comparison, the experimental values<sup>20</sup> are  $C_{11} = 114 \text{ GPa}$ ,  $C_{12} = 62 \text{ GPa}$  and  $C_{44} = 32 \text{ GPa}$ , and LDA calculations<sup>17,21</sup> predict  $a_0 = 3.98 \text{ \AA}$ ,  $E_{\text{coh}} = 4.15 \text{ eV}$ ,  $C_{11} = 135 \text{ GPa}$ ,  $C_{12} = 70 \text{ GPa}$  and  $C_{44} = 35 \text{ GPa}$ .

### 2. Diffusion barriers

Diffusion is central to many physical processes which determine the morphology of surfaces, such as step flow, nucleation, and growth.<sup>22</sup> It is of obvious importance to study diffusion processes theoretically, since direct observations of surface diffusion by means of field ion microscopy (FIM)<sup>23</sup> are limited to a few surfaces due to the response limits of the materials of interest to high voltages.<sup>22</sup> The barriers for single adatom diffusion on Al surfaces calculated by Stumpf and Scheffler<sup>15-17</sup> using *ab initio* LDA techniques, provide a stringent test for the present empirical Al-Al interaction model. It is generally accepted that diffusion on flat metal surfaces proceeds by either hopping or exchange.<sup>24</sup> In the two following subsections compare the results of the present model for these mechanisms with previous LDA results.

*Hopping Diffusion* – During hopping diffusion the adatom is moving between minima of the potential energy surface, *i.e.* between stable or metastable binding sites. On the (111) surface the stable adsorption sites are the 3-fold fcc and hcp sites; on the (100) surface there is single independent adsorption site, the four-fold hollow; the (110) surface is analogous, with a five-fold site. Hopping diffusion on the (110) surface is intrinsically anisotropic, since it can proceed perpendicular or parallel to the  $[1\bar{1}0]$ -oriented atomic rows, respectively via the short bridge or long bridge paths. The activation energies for the long and short bridge are labelled  $E_{\parallel}$  and  $E_{\perp}$  respectively.

For each surface we performed total energy calculations for the adatom sitting at the adsorption site and at the bridge site. At the latter site the total energy is minimized with respect to distance of the adatom from surface. All other Al positions are fully optimized. The energy difference between adsorption and bridge site is

defined to be the activation energy for hopping diffusion. Further technicalities are discussed in the Appendix. Table V summarizes the activation energies for surface self diffusion obtained with the present model and compares the barrier heights to results from previous *ab initio* calculations. The barrier for diffusion on Al (111) was used to set up the potential, hence it agrees with LDA results by construction. On Al (100), we obtain a diffusion barrier in good agreement with first principle calculations; we are not aware of experimental results for these self-diffusion barriers on Al(111) and Al(100). According to a recent study,<sup>25</sup> the hopping-self-diffusion barriers calculated *ab initio* in the generalized gradient approximation to density functional theory for unreconstructed fcc(100) surfaces equal one sixth the bulk cohesive energy; this is found to be the case for Al also in our calculations. In the case of Al (110), the present potential correctly predicts diffusion anisotropy, although some quantitative discrepancy exists with the predictions of *ab initio* calculations.<sup>15,16</sup> FIM studies<sup>23</sup> find no anisotropy for the diffusion on the (110) surface, and report a barrier height of 0.43 eV for both paths. This discrepancy with our result is due to the fact that here we only addressed hopping diffusion for demonstrative purposes. In fact, exchange diffusion normal to the rows is known to have a barrier as low as  $\simeq 0.6 \text{ eV}$ ,<sup>15,16</sup> which restores a reasonable agreement with experiment.

*Exchange Diffusion* – Diffusion by atomic exchange occurs as the adatom replaces a surface atom, which in turn pops up at an adjacent stable surface site. Diffusion by exchange was discussed by Bassett and Webber<sup>26</sup> and Wrigley and Ehrlich<sup>27</sup>, and predicted theoretically for (100) surfaces by Feibelman.<sup>28</sup> This diffusion mode can lower significantly the effective diffusion barriers. Views on why diffusion by exchange is favorable for some metal surfaces is discussed in Refs. 17, 28, 29, 30, and references therein. For Al (100), we calculated the activation energy for exchange diffusion (see Table V) and found it lower than for hopping, as do first-principles calculations. The quantitative agreement is reasonably good.

### 3. Surface and step energies

The surface energy, defined as the difference between the energy of an atom at the surface and in the bulk environment, is usually calculated as

$$E_{\text{surf}}^{\text{area}} = \frac{E_{\text{slab}} - N E_{\text{bulk}}}{2A} \quad (8)$$

$$E_{\text{surf}}^{\text{atom}} = \frac{E_{\text{slab}} - N E_{\text{bulk}}}{2N_{\text{surf}}} \quad (9)$$

where  $E_{\text{slab}}$  is the total energy of the slab,  $N$  the total number of atoms in the slab,  $N_{\text{surf}}$  the number of atoms on each surface,  $E_{\text{bulk}}$  is the total energy per bulk atom,  $A$  is the area of each free surface of the slab, and the factor 1/2 accounts for the two free surfaces of the simulation cell; periodic boundary conditions are applied in

the planar directions. These formulas are not problem-free in general,<sup>31</sup> but we have checked that they are in the cases of interest to us.

We calculated the formation energies for the low index (111), (100) and (110) Al surfaces with the present Al-Al interaction model. The comparison of our results to those obtained in *ab initio* LDA investigations, given in Table VI shows that the trends of surface energies of our Al model are consistent with the *ab initio* calculations. We obtain all surface energies about 20% lower than the LDA surface energies. Keeping in mind the known LDA overestimate of the binding energies (the LDA cohesive energy of Al is 1.15 eV<sup>16</sup>), about 20% larger than the experimental value (0.93 eV) the agreement between the two models is excellent.

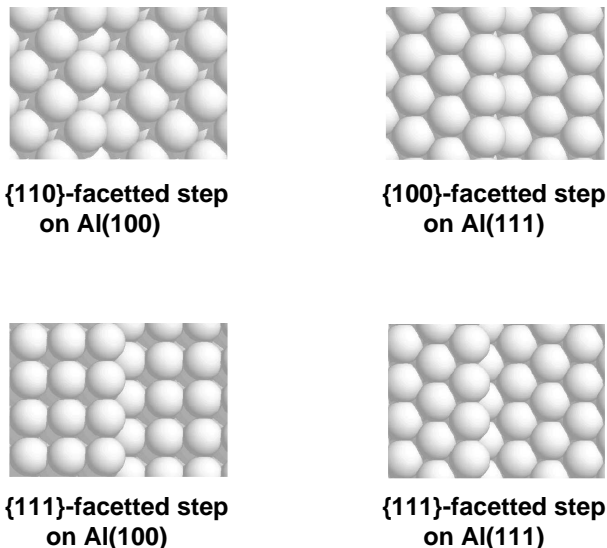


FIG. 1. Atomic arrangement of the {110} and {111} faceted steps on Al (100), and the {100} and {111} faceted step on Al (111).

The energy per unit length of a step on a low-index surface is defined in terms of the energies of the low-index surface and the vicinal surface used to simulate the step itself, and of the geometrical parameters thereof:<sup>32</sup>

$$E_{\text{step}} = d_{s-s} E_{\text{vicinal}} - l_{\text{terrace}} E_{\text{low-index}}, \quad (10)$$

with  $d_{s-s}$  the step-step distance, and  $l_{\text{terrace}}$  the terrace length on the vicinal surface. In analogy to the surface energy, the step energy can also be expressed per step atom.

Although a stepped vicinal surface can be specified by its corresponding Miller indices, this notation is not very convenient, as it does not indicate at first sight the geometrical structure of the surface. Thus we use instead the notation  $[n(h, k, l) \times m(h', k', l')]$  by Lang *et al.*,<sup>33,34</sup> where  $(h, k, l)$  and  $(h', k', l')$  are the Miller indices of the terraces and ledges respectively;  $n$  gives the number of atomic rows in the terrace parallel to the step, and  $m$

corresponds to the height of the step. In the case of monoatomic-height steps,  $m$  is omitted in this notation.

For the two low index surfaces Al (100) and Al (111), we calculated the formation energy of different steps. On Al (100) there exist two monoatomic steps, the close-packed {111}-faceted and the more open {110}-faceted. The former belongs to the family of  $(1, 1, 2n+1)$ -surfaces, the latter to the family of the  $(1, 0, n)$ -surfaces.<sup>35,36</sup> For the calculation of the step energies we used the Al(1, 1, 15) = Al[9(100) × (111)] and the Al(1, 0, 9) = Al[9(100) × (110)] surfaces.

On Al(111) there are two types of close-packed steps, the {111}-faceted and the {100}-faceted. The corresponding vicinal surfaces belong to the  $(n, n, n-2)$  and  $(n, n, n+2)$  families, respectively. We used the Al(9, 9, 7) = Al[9(111) × (111)] and the Al(8, 8, 10) = Al[9(111) × (100)] surfaces. The geometry of the different steps on the Al(100) and Al (111) surface is depicted in Fig.1. For all these vicinals, the terraces separating the steps have the same width of 9 atomic rows. We have verified that step-step repulsion at these inter-step distances is already in the long-range elastic regime  $\sim d_{s-s}^{-2}$ ,<sup>32,37</sup> the steps are far enough to extract their formation energy without an unknown bias from the interstep interaction.

Table VII lists the results for step formation energies, and compares them to *ab initio* data. The empirical Al potential describes the step formation energies for the two different steps on Al (111) in excellent agreement with first-principles calculations. More energy is needed to create steps on the close-packed Al (111) surface than on the more open Al (100). The open step on the Al (100) surface has a 20% larger formation energy than the close-packed step, in agreement with bond cutting arguments.<sup>38</sup>

#### 4. The Al Dimer

The dimer is a stringent test for an Al-Al interaction model, since atoms in a dimer experience a very different chemical environment compared to bulk or surface atoms. For Al<sub>2</sub>, our model yields a binding energy per atom of 0.70 eV and a bond length of 2.70 Å. The binding energy was indeed used as input to determine the model parameters, matching the LDA value<sup>39</sup> of 0.71 eV ( $-0.68 \pm 0.03$ eV experimental, Ref. 40) The lowest vibrational frequency is calculated to be  $\nu = 290 \text{ cm}^{-1}$ , in excellent agreement with the experimental value<sup>41</sup> of  $284.2 \text{ cm}^{-1}$ . The predicted bond length of our model matches exactly the experimental estimate.<sup>41</sup> Thus, the present model describes satisfactorily the bonding of Al in the rather extreme case of the Al<sub>2</sub> dimer.

As the understanding of diffusion and growth requires a knowledge of the binding energies of small aggregates of adatoms, we also calculated the energy of two Al adatoms sitting at neighboring fcc sites on an Al (111) surface. The energy gain with respect to isolated adatoms is 0.50

eV, *i.e.* the Al ad-dimer is stabilized appreciably over separated adatoms. LDA calculations<sup>17</sup> yield a similar energy gain of 0.58 eV.

### 5. Sticking coefficient for hyperthermal Al atoms

During physical vapor deposition the Al atoms emitted from the sputter source have a non-thermal energy distribution, with kinetic energies exceeding 10 eV. Therefore the sticking coefficient, a key ingredient for a reliable modelling of metal film growth, cannot be assumed to be constant and independent of the particle’s energy as it is typically done. In order to elucidate the dependence of the sticking coefficient on impingement energy, we start our simulations with the incident Al atom placed outside the interaction range of the surface. Its initial kinetic energy is set in the range of 0 to 125 eV, and its starting angle off the surface normal in the range 0° to 60°, which corresponds to typical ionized physical vapor deposition conditions. The trajectories of the incident atom, and of any other atom which may be etched away from the surface upon impact, are monitored until either a certain time span has elapsed, or the outgoing atoms (in the case of reflection or etching) have traveled a distance of 10 Å away from the surface. Analyzing 200 trajectories per incident energy and angle, we collected a statistically significant sample of well-defined adsorption, reflection, and etching events. The relative probability of the sticking coefficient is calculated as the ratio of the number of adsorption events to the total number. The typical statistical error in the reaction probability thus determined is below 5 %. Fig.2 depicts the sticking coefficient as a function of energy for Al atoms impinging normally on the surface (solid circles) or at an off-normal angle of 40° (open circles).

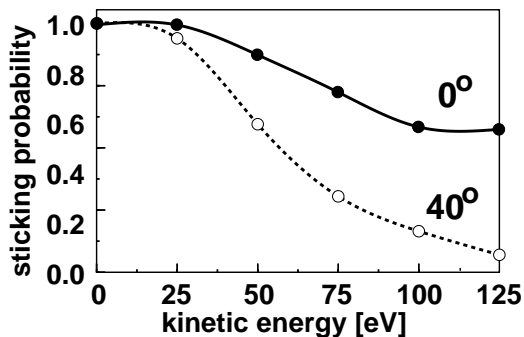


FIG. 2. Sticking probabilities for hyperthermal Al atoms impinging on an Al (111) surface. As a function of kinetic energy the solid line with filled circles depicts the reaction probabilities for Al atoms impinging normal on the surface and the dashed line with the open circles show the latter quantity for an angle of 40° to the normal.

The sticking probability varies strongly with the inci-

dent kinetic energy; the angle to the normal also has a drastic effect. Details of the molecular dynamics calculations are given in Sec.A 2. Further discussion and results on high energy deposition are reported in Ref. 42.

## III. APPLICATION: FREE ENERGY CALCULATIONS

In this applicative Section of the paper, we compare surface free energies of Al computed using different levels of quasi-harmonic approximation, and thermodynamic integration via Monte Carlo simulations. The latter effectively functions as “exact” reference for the various harmonic approximation. Before presenting the results, we briefly review the background theory of the different approaches.

### A. Theory

*Thermodynamic Integration* – The free energy cannot be calculated as an ensemble average.<sup>43</sup> The method of thermodynamic integration<sup>10,43–47</sup> circumvents this problem starting from the concept of Stockmayer fluid, a fictitious system in which the interparticle interaction potential  $U_\lambda$  is gradually switched on from a known reference potential  $U_h$  to the actual, full interaction potential  $U$ ; the mixing of  $U_h$  and  $U$  into the effective potential is controlled by a parameter  $\lambda$ :

$$U_\lambda = (1 - \lambda)U_h + \lambda U. \quad (11)$$

The key relation of the method concerns the derivative of  $F$  with respect to  $\lambda$ :

$$\frac{dF}{d\lambda} = \left\langle \frac{dU_\lambda}{d\lambda} \right\rangle_\lambda = \langle U - U_h \rangle_\lambda. \quad (12)$$

The subscript  $\lambda$  means that the average has to be evaluated with the interaction potential  $U_\lambda$ . Integrating the latter equation one arrives at the following expression for the free energy of the system of interest:

$$F_{\lambda=1} = F_{\lambda=0} + \int_0^1 \langle U - U_h \rangle_\lambda d\lambda \quad (13)$$

The usual choice for the reference system is the Einstein crystal (*i.e.* a system of non-interacting harmonic oscillators with the interaction potential  $U_h = \frac{1}{2}m\omega_D \sum_i |\mathbf{r}_i - \mathbf{r}_{i0}|^2$ ), whose free energy is

$$F_{\lambda=0} = -3Nk_B T \ln \left( \frac{T}{\Theta_D} \right), \quad (14)$$

with  $\Theta_D$  the Debye temperature (394 K for Al<sup>48</sup>). The free energy of the real system can thus be obtained at any given temperature by a series of canonical Monte Carlo simulations.

A faster way to obtain the temperature variation of the free energy is to integrate the thermodynamical relation

$$\frac{d}{dT} \left( \frac{F}{T} \right) = - \left\langle \frac{H}{T^2} \right\rangle, \quad (15)$$

from a reference temperature upwards. This requires a simple (*e.g.*) Monte Carlo ensemble average of the energy for each temperature, and of course a reference value of  $F$  from thermodynamic integration.

In summary, the free energy of the system at a reference temperature  $T_0$  is determined with Eq.(13); then, the temperature variation from  $T_0$  to  $T$  is calculated using Eq.(15). Both steps were performed by canonical Metropolis Monte Carlo simulations.<sup>43,49</sup> As detailed below, thermal expansion is taken into account performing the NVT Monte Carlo calculations at the temperature-dependent lattice constant determined independently by NPT molecular dynamics.

*Quasi-harmonic approach* – A popular approach to free energy calculations is the quasi-harmonic approximation. Thereby, the full interatomic potential is replaced by its quadratic expansion about the atomic equilibrium positions. The system is then equivalent to a collection of harmonic oscillators, and diagonalization of the corresponding dynamical matrix yields the squares of the normal-mode frequencies, *i.e.* the phonon spectrum. In bulk systems the dynamical matrix is a  $3 \times 3$  matrix; for a slab system it is a  $3\ell \times 3\ell$  matrix, where  $\ell$  is the number of atomic layers in the slab. The dynamical matrix is given by<sup>50</sup>

$$D_{\alpha\beta}(\ell \ell') = \frac{1}{m} \sum_{\ell''} \Phi_{\alpha\beta}(\ell \ell'') \exp[i\mathbf{q}(\mathbf{r}_0 - \mathbf{r}_0'')] \quad (16)$$

where the force constant matrix  $\Phi_{\alpha\beta}(\ell \ell')$  is defined as

$$\Phi_{\alpha\beta}(\ell \ell') = \left( \frac{\partial^2 U}{\partial u_\alpha(\ell) \partial u_\beta(\ell')} \right)_0. \quad (17)$$

The subscript "0" indicates that the second derivatives are to be evaluated at the true mean positions of the atoms, with any displacements from the bulk positions (*e.g.* surface relaxations or reconstructions) taken into account. The equilibrium positions  $x_0^\ell, y_0^\ell, z_0^\ell$  of the atoms are given by the vectors  $\ell = (\ell_1, \ell_2, \ell_3)$ ; the  $\ell_3$  axis is perpendicular to the surface and the position of an atom within a plane is specified by  $\ell_1, \ell_2$ , and  $u_\alpha(\ell)$  describes the  $\alpha$  component ( $\alpha = x, y, z$ ) of the position of the  $\ell$ -th atom from its mean position  $x_0^\ell, y_0^\ell, z_0^\ell$ .

The phonon spectrum of bulk Al and of Al (100) are displayed in Fig.3, upper and lower panels respectively (for both calculations supercells comprising 50 layers stacked along (100) have been employed). A variety of surface modes appear in bulk gaps or split off from bulk band edges. These additional modes are the source of the different vibrational free energy of surface systems in comparison to bulk systems. The free energy in this

approximation is calculated for lattice and geometrical parameters  $\mathbf{a}$  at temperature  $T$  as

$$F(\mathbf{a}, T) = E_0(\mathbf{a}) + k_B T \sum_{\mathbf{k}, j} \ln \left( 2 \sinh \frac{\hbar \omega_j(\mathbf{k})}{2k_B T} \right). \quad (18)$$

The sum runs over all phonon polarizations  $j$  and wave vectors  $\mathbf{k}$  in the Brillouin zone, with  $\omega_j(\mathbf{k})$  the frequency of the corresponding modes. Both the frequencies, and the internal energy  $E_0(\mathbf{a})$  of the ideal static lattice, depend on all the lattice and geometrical parameters  $\mathbf{a}$ . The latter include the bulk lattice constant and, for the surface, the additional geometrical parameters involved in relaxations or reconstructions.

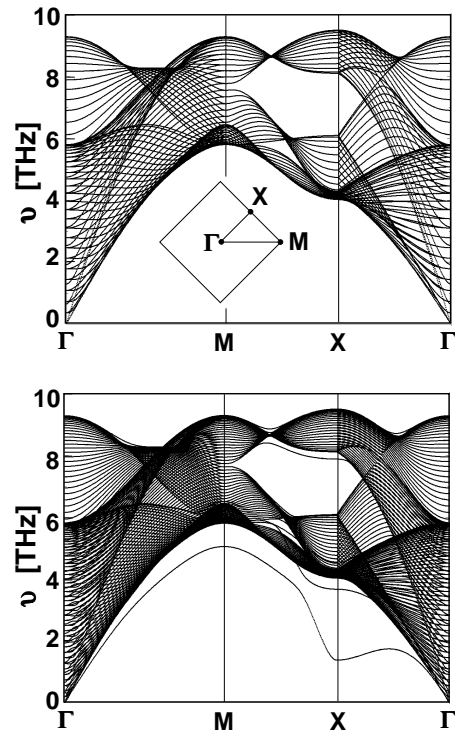


FIG. 3. Bulk (a) and surface (b) phonon spectra for Al calculated with a 50 layer slab. In (b) the slab has two (100) surfaces, the frequencies are plotted along lines of high symmetry. The corresponding 2d-Brillouin zone is shown in the inset of panel (a).

In a bulk system the forces on each atom are zero by symmetry, independently of  $a$ , so that it is strictly correct to neglect the first derivatives in the quadratic expansion of the potential energy. We have verified that the quasi-harmonic approximation does indeed work very well for the bulk even in comparison to thermodynamic integration. For a surface, the situation is different, since the interlayer spacings (especially those of the top surface layers) will change with respect to the bulk, *i.e.* the surface will generally either contract or expand. The average equilibrium positions of the near-surface layers (the interlayer spacings in the case of simple relaxation) are determined by the minimum of the free energy, but that

is, of course, unknown a priori. In addition, the harmonic expansion is not strictly correct (since the forces, *i.e.* the derivatives of the internal potential energy are not zero at the free energy minimum), which is why one calls this the quasi-harmonic approximation to begin with. In fact, it is clear that there are several levels of approximation possible for the quasi-harmonic approach; here we consider some of those:

1. The computationally simplest way is to optimize the atomic configuration and calculate the phonons *at zero temperature*, and evaluate the free energy vs.  $T$  using those ingredients for all  $T$ . Within this approach, the quasi-harmonic approximation is strictly valid, as we expand the potential energy function around the equilibrium positions, and the  $T$  dependence enters solely with Eq.(18). In real systems, of course, both the surface internal energy *and* the vibrational contribution to the free energy will change with  $T$ , but it is a priori unclear to what degree this influences the result.
2. Another way to account for the effects of finite temperature is to take the  $T = 0$  atomic positions, rescale their coordinates as a function of the temperature according to the appropriate bulk thermal expansion coefficient, and recalculate the phonons (and hence the free energy) for the expanded lattice. This is a hybrid case in which  $T$  not only affects the force constants, but also the surface internal energy. Of course it is arbitrary to use the scaled  $T=0$  interlayer spacings at non-zero temperatures. Also, it should be kept in mind that the harmonic approximation is not strictly valid for the expansion of the potential energy around non-equilibrium positions.
3. A further possibility is to rescale all the coordinates according to thermal expansion first, and then re-optimize all atomic positions; the phonons and the free energy are calculated for that geometry. Here one is consistent with the prerequisites of the quasi-harmonic expansion, but at the cost of getting wrong interlayer spacings at the surface.
4. The real thing is of course to minimize the total free energy with a “self-consistent” adjustment of the atomic positions of all layers in the slab system, resulting in the thermodynamic equilibrium configuration of the surface system. In practice, one starts with the bulk positions rescaled according to thermal expansion, and then adjusts the interlayer spacings of a few near-surface layers to obtain the minimum of the free energy. The major contribution is generally due to the first two surface layers, the only having a sizable displacement from the bulk interlayer spacing. In our calculations, we therefore changed  $d_{12}$  by  $\pm 3\%$  and  $d_{23}$  by  $\pm 2\%$ .

## B. Results

We now compare the free energy of an Al(100) surface calculated within the different quasi-harmonic approaches (1–4) described above, with the results of thermodynamic integration; the latter effectively functions as exact reference since it takes the full potential into account, hence in particular all anharmonic contributions. We chose the (100) surface for demonstrative purposes, as intermediate between the closed packed (111) and the more open (110) surface.

### 1. Comparison of different methods

In order to obtain the bulk lattice constant at different temperatures we first performed zero-pressure molecular dynamics simulation<sup>49,51,52</sup> using our Al potential. In the linear regime the expansion coefficient is  $\alpha = 1.64 \times 10^{-5} \text{ \AA/K}$ , the experimental value being  $2.36 \times 10^{-5} \text{ \AA/K}$ .<sup>53</sup> Deviations from linearity set in<sup>54</sup> at about 500 K. The dimensions of the simulation cell with periodic boundary conditions correspond, in all subsequent calculations, to the bulk lattice constant at the relevant temperature. The surface free energy calculations imply the evaluation of the bulk free energy, and of the free energy of a slab system with two surfaces. The surface free energy is then determined with Eq.(9).

In Fig.4 we compare the surface free energy calculated with thermodynamic integration and the quasi-harmonic approach. All versions of the latter underestimate severely the temperature variation of the surface free energy. This is mainly due to the neglect of anharmonicity, which is also responsible for thermal expansion. A first important result is then that at temperatures  $T \geq \Theta_D$ , the harmonic approximation is inappropriate for Al surfaces.

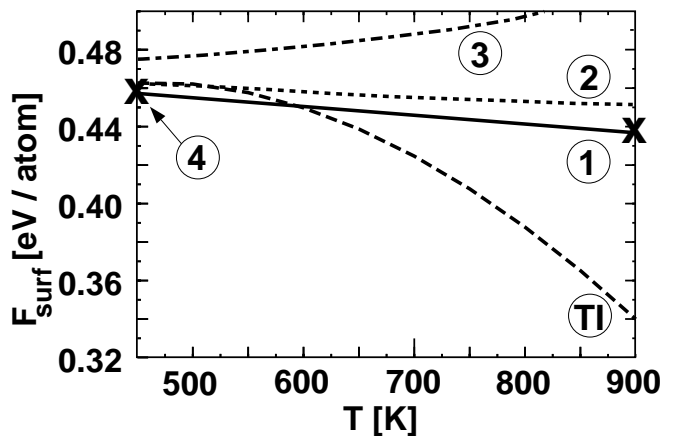


FIG. 4. Surface free energies for Al (100) calculated with different quasi-harmonic approaches (as discussed in the text) and with the method of thermodynamic integration. Solid line: approach (1), zero-temperature phonons for all temperatures; dotted line: approach (2), positions rescaled according to thermal expansion; dash-dotted line: approach (3), as (2) with re-optimization of atomic positions; crosses: approach (4), minimization of the free energy in the  $\{d_{12}, d_{23}\}$  plane; dashed line: (TI) thermodynamic integration, reference for harmonic approximations. See text for more details.

Note that the failure of the harmonic approximation for the present relatively high-temperature calculations does not affect the successes of this approach at low temperatures, an example being the recent first-principles calculations for Be surfaces.<sup>55</sup> The reason why those results are compatible with ours is clearly that we work well above the Debye temperature of our system ( $\sim 400$  K), whereas the highest temperature considered in Ref. 55 is 750 K, well below  $\Theta_D^{\text{Be}} \simeq 1000$  K (as extracted from a Debye-Einstein model). Of course, the quasi-harmonic approach will generally fail if applied to systems at sufficiently high temperatures.

To sort out the relative merits of the various levels of harmonic approximation, we focus on the effects of the interlayer spacing  $d_{12}$  (between first and second layer) and  $d_{23}$  (between second and third layer) on the surface energy and on the vibrational contribution to the surface free energy. Essentially this is the fourth level of approximation mentioned earlier. We pick  $T=450$  K for demonstrative purposes, and expand the lattice accordingly.

Panel (a) in Fig.5 shows the variation of the plain surface energy as a function of the interlayer spacings (expressed in turn in percentage of the bulk interlayer spacing). An increase of the interlayer spacings tends to increase the energy drastically, a decrease to reduce it. The minimum at around  $-3\%$  for both spacings. These fairly unrealistic values result from the optimization of the interlayer spacing for a laterally expanded surface.

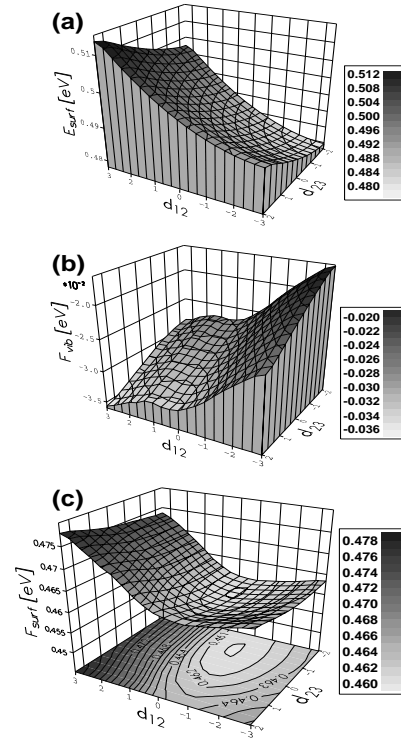


FIG. 5. Panel (a): dependence of the plain surface energy on the interlayer spacing  $d_{12}$  and  $d_{23}$ . Panel (b): vibrational contribution to the surface free energy as a function of the interlayer spacings. Panel (c): total surface free energy, sum of the two previous contributions.

The excess surface free energy, *i.e.* the vibrational contribution is shown in panel (b) of Fig.5. An increase of the interlayer spacings leads to softer force constants and hence to lower frequencies, which yield according to Eq.(18) a more negative value of the surface excess free energy. The dependence on the first spacing is stronger than on the second, although conceptually both spacings would tend to positive infinity (decoupled Al planes) if only the vibrational contribution mattered.

The opposing tendencies of the internal and vibrational contributions tend to compensate; in fact, summing up the plain surface energy and the vibrational contribution, one arrives at the total surface free energy depicted as a function of the interlayer spacings in panel (c) of Fig.5. For the Al (100) surface, the minimum in the free energy corresponds to  $d_{12} = -0.5\%$  and  $d_{23} = -0.9\%$ , a compromise between the gain of free energy upon outward relaxation, and that in plain surface energy upon inward relaxation.

In approaches (1) and (2) from our above list (force constants from zero-temperature or rescaled zero-temperature positions), the interlayer spacings are  $d_{12} = -1.5\%$  and  $d_{23} = -1.3\%$ . These are rather close to the minimum of the free energy found by direct minimization in approach (4); indeed, with reference to Fig.4, both approach (1) (solid line) and (2) (dashed line) match rather closely the values of approach (4) (crosses), *i.e.* of the full



quasi-harmonic calculation. Approach (3) (dash-dotted line), where we rescaled the lattice constant and then re-optimized all atomic positions, fails badly, going astray already near the Debye temperature, and progressively more so for higher temperatures. This is due to the incorrect (free-energy-wise) spacings imposed on the near-surface layers by the minimization of the internal energy. The spacings are found to be  $d_{12}=-3.4\%$  and  $d_{23}=-3.1\%$  at 450 K, and  $d_{12}=-5.8\%$  and  $d_{23}=-5.5\%$  at 900 K. A glance at panel (c) of Fig.5 reveals that both of these points in the  $\{d_{12}, d_{23}\}$  plane do indeed correspond to free energies very far away from the minimum (especially at the higher temperature).

In conclusion, the most naive and simplest approach of exporting the  $T = 0$  force constants and surface energy to non-zero temperature does indeed underestimate considerably the temperature variation of the surface free energy with respect to thermodynamic integration, but it gives an agreement comparable to, or better than the sophisticated adjustment of the interlayers to find the free energy minimum.

#### IV. SUMMARY

We have presented a refined Al interatomic potential for classical dynamics and Monte Carlo simulations. We thoroughly tested its functionalities, finding it to be very accurate for a variety of systems. Next, we applied it to evaluating the performance of quasi-harmonic approaches to free energy calculations for surfaces, comparing the latter results with full thermodynamic integration results. For Al surfaces, the quasi-harmonic approximation shows a progressively increasing error for temperatures above  $\Theta_D$ . Different levels of quasi-harmonic approximation have been compared; for Al, the simplest method of using zero-temperature phonons to compute the free energy at all temperatures is as accurate as the explicit minimization of the free energy with respect to geometrical parameters.

#### ACKNOWLEDGMENTS

We thank Dr. Furio Ercolessi for helpful assistance. U. Hansen and P. Vogl acknowledge financial support by Siemens AG. V. Fiorentini was supported by the Alexander von Humboldt-Stiftung during his stay at the Walter Schottky Institut.

#### APPENDIX A: COMPUTATIONAL DETAILS

##### 1. Substrate sizes

For the calculation of the surface self-diffusion barriers, and surface and step energies, we have employed finite

slabs with periodic boundary conditions for the lateral cells. The supercells contained of 672, 550 and 560 atoms for the Al(111), Al(100) and Al(110) surfaces and consisted of 12, 11 and 9 atomic layers. In order to determine the surface energies of Al(111), Al(100) and Al(110) the supercells contained 1080, 550 and 560 atoms, arranged in 9, 11 and 16 atomic layers. The step formation energies were obtained from systems containing 4 steps and 72, 105, 102 and 102 atoms per layer corresponding to a total number of 1312, 2724, 1368 and 2532 atoms for the Al(1, 0, 9), Al(1, 1, 15), Al(8, 8, 10) and Al(9, 9, 7) surface. All forces  $\mathbf{F}$  per atom have been brought below a threshold of  $10^{-5}$  eV/Å. We estimated the errors in the total energies due to the finite supercell size to be well below  $10^{-4}$  eV/atom.

##### 2. Molecular dynamics calculation of the sticking probability

The reaction probabilities were calculated in classical molecular dynamics simulations using our Al interaction potential. The integration was performed with a 5-th order Runge Kutta method with an adaptive timestep, in order to ensure total energy conservation throughout the simulation. Supercells containing 1320 atoms arranged in 10 atomic layers were employed; cell dimensions are chosen so as to avoid artifacts of the in-plane periodicity. The starting configuration is chosen to be a (111) surface, the one Al surface with the lowest formation energy. All atomic coordinates are allowed to evolve dynamically, except those of the two bottom layers of the supercell. The surface temperature is set at 450 K (i.e about 1/2 of the melting temperature, and  $\sim 15\%$  larger than the bulk Debye temperature).

##### 3. Monte Carlo calculations within the canonical ensemble

All Monte Carlo calculations were performed within the canonical ensemble, using the standard Metropolis technique.<sup>43,49</sup> The maximum atomic displacement was automatically adjusted in order to get an acceptance ratio of 0.4. It was not systematically studied that this acceptance ratio was an optimum, but well converged statistical averages were obtained with a typical number of Monte Carlo moves of order  $10^4$  times the number of atoms in the system. Before averaging, the system was equilibrated for a number of steps of order 500 times the number of atoms in the system. For the Al (100) surface we used in total 384 atoms.

#### 4. Quasi-Harmonic free energy calculations

Within the quasi-harmonic methods we employed slab geometries with 20 atomic layers each containing 32 atoms. For the  $\mathbf{k}$ -space summation we used grids typically containing 2500 equally spaced  $\mathbf{k}$ -points. Careful tests showed that this number of  $\mathbf{k}$ -points yields well converged results.

- 
- <sup>1</sup> S. Valkealahti and M. Manninen, J. Phys.: Condens. Matter **9** 4041, 1997.
- <sup>2</sup> S. J. Zhou, P. S. Lomdahl, R. Thomson and B. L. Holian, Phys. Rev. Lett. **76**, 2318 (1997).
- <sup>3</sup> D. J. Harris, G. W. Watson and S. C. Parker, Phys. Rev. B **56**, 11477 (1997).
- <sup>4</sup> A. F. Voter, in *Interatomic Potentials for Atomistic Simulations*, MRS Bulletin **21**, 17 (1996).
- <sup>5</sup> W. F. van Gunsteren and A. E. Mark, J. Chem. Phys. **108**, 6109 (1998).
- <sup>6</sup> Y. P. Liu, K. Kim, J. Berne, R. A. Friesner and S. W. Rick, J. Chem. Phys. **108**, 4739 (1998).
- <sup>7</sup> J. Cai and Y. Y. Ye, Phys. Rev. B **54**, 8398 (1996).
- <sup>8</sup> R. G. Hoagland, M. S. Daw, S. M. Foiles, and M. I. Baskes, J. Mater. Res. **5**, 313 (1990).
- <sup>9</sup> M. I. Baskes, Phys. Rev. B **46**, 2727 (1992).
- <sup>10</sup> J. Mei and J. W. Davenport, Phys. Rev. B **46**, 21 (1992).
- <sup>11</sup> M. S. Daw and M. I. Baskes, Phys. Rev. B **29**, 6443 (1984).
- <sup>12</sup> M. S. Daw and M. I. Baskes, Phys. Rev. Lett. **50**, 1285 (1983).
- <sup>13</sup> M. J. Stott and E. Zaremba, Phys. Rev. B **22**, 1564 (1980).
- <sup>14</sup> F. Ercolessi and J. B. Adams, Europhys. Lett. **26**, 583 (1994).
- <sup>15</sup> R. Stumpf and M. Scheffler, Surf. Sci. **307**, 501 (1994).
- <sup>16</sup> R. Stumpf and M. Scheffler, Phys. Rev. Lett. **72**, 254 (1994).
- <sup>17</sup> R. Stumpf and M. Scheffler, Phys. Rev. B **53**, 4958 (1996).
- <sup>18</sup> C. L. Liu, J. M. Cohen, J. B. Adams, and A. F. Voter, Surf. Sci. **253**, 334 (1991).
- <sup>19</sup> A. A. Abrahamson, Phys. Rev. **178**, 178 (1969).
- <sup>20</sup> G. N. Kamm and G. A. Alers, J. Appl. Phys. **35**, 327 (1964).
- <sup>21</sup> V. B. Deyirmenjian, V. Heine, M. C. Payne, V. Milman, R. M. Lynden-Bell, and M. W. Finnis, Phys. Rev. B **52**, 15191 (1995).
- <sup>22</sup> G. Boisvert, L. J. Lewis, M. J. Puska, and R. M. Nieminen, Phys. Rev. B **52** 9078, 1995.
- <sup>23</sup> G. L. Kellogg, Surf. Sci. Rep. **21**, 1994.
- <sup>24</sup> G. L. Kellogg, Phys. Rev. Lett. **76**, 98, 1996.
- <sup>25</sup> P. J. Feibelman, Surf. Sci. **423**, 169 (1999).
- <sup>26</sup> D. W. Bassett and P. R. Weber, Surf. Sci. B **70**, 520, 1978.
- <sup>27</sup> J. D. Wrigley and G. Ehrlich, Phys. Rev. Lett. **44**, 661 (1980).
- <sup>28</sup> P. J. Feibelman, Phys. Rev. Lett. **65**, 729 (1990).
- <sup>29</sup> B. D. Yu, M. Scheffler, Phys. Rev. B **56**, 15569, 1997.
- <sup>30</sup> P. J. Feibelman and R. Stumpf, Phys. Rev. B **59**, 5892 (1999).
- <sup>31</sup> V. Fiorentini and M. Methfessel, J. Phys.: Condensed Matter **8**, 6525 (1996)
- <sup>32</sup> R. Najafabadi, D. J. Srolovitz, Surf. Sci. **317**, 221 (1994).
- <sup>33</sup> B. Lang, R. W. Joyner, and G. A. Somorjai, Surf. Sci. B **30**, 440, 1972.
- <sup>34</sup> M.-C. Desjonqueres and D. Spanjaard, *Concepts in Surface Science* (Springer, Berlin, 1993)
- <sup>35</sup> D. R. Eisner and T. L. Einstein, Surf. Sci. **286**, L559, 1993.
- <sup>36</sup> M. A. Van Hove and G. A. Somorjai, Surf. Sci. B **92**, 489, 1980.
- <sup>37</sup> L. E. Shilkrot and D. J. Srolovitz, Phys. Rev. B **53**, 11120 (1996).
- <sup>38</sup> M. Methfessel, D. Hennig, and M. Scheffler, Appl. Phys. A **55**, 442 (1995), and references therein.
- <sup>39</sup> I. J. Robertson, V. Heine, and M. C. Payne, Phys. Rev. Lett. **70**, 1944 (1993).
- <sup>40</sup> Z. Fu, G. W. Lemire, G. A. Bishea and M. D. Morse, J. Chem. Phys. **93**, 8420 (1990).
- <sup>41</sup> M. F. Cai, T. P. Djugan, and V. E. Bondybey, Chem. Rev. Lett. **155**, 430 (1989).
- <sup>42</sup> U. Hansen, P. Vogl, and V. Fiorentini, Phys. Rev. **59**, R7856 (1999).
- <sup>43</sup> D. Frenkel and B. Smit, *Understanding Molecular Simulations: From Algorithms to Applications* (Academic Press, Boston 1996).
- <sup>44</sup> S. M. Foiles and J. N. Adams, Phys. Rev. B **40**, 5909 (1989).
- <sup>45</sup> S. M. Foiles, Phys. Rev. B **49**, 14930 (1994).
- <sup>46</sup> J. R. Morris, C. Z. Wang, K. M. Ho and C. T. Chan, Phys. Rev. B **49**, 3109, 1994.
- <sup>47</sup> M. J. Vlot and J. van der Eerden, J. Chem. Phys. **106**, 2771, 1997.
- <sup>48</sup> J. de Launay, in *Solid State Physics*, Vol. 2, F. Seitz and D. Turnbull eds. (Academic Press, New York, 1956).
- <sup>49</sup> M. P. Allen D. J. Tildesley, *Computer Simulation of Liquids* (Oxford UP, Oxford 1996).
- <sup>50</sup> R. E. Allen and F. W. de Wette, Phys. Rev. **179**, 873 (1969).
- <sup>51</sup> H. J. C. Berendsen, J. P. M. Postma, W. F. van Gunsteren, A. DiNola and J. R. Haak, J. Chem. Phys. **81**, 3684, 1984.
- <sup>52</sup> G. J. Martyna, D. J. Tobias and M. L. Klein, Mol. Phys. **87**, 117, 1996.
- <sup>53</sup> W. B. Pearson, in *Handbook of Lattice Spacings and Structures of Metals and Alloys* (Pergamon Press, New York, 1958).
- <sup>54</sup> The thermal expansion of the lattice constant is well described for  $0 < T < 950$  K by  $a(T) = a_0 + \alpha_1 T + \alpha_3 T^3$ , where  $a_0 = 4.032$  Å,  $\alpha_1 = 6.35 \times 10^{-5}$  Å/K and  $\alpha_3 = 1.26 \times 10^{-11}$  Å/K<sup>3</sup>.
- <sup>55</sup> M. Lazzeri and S. de Gironcoli, Phys. Rev. Lett. **81**, 2096 (1998).

TABLE I. Parameters used to define the atomic density function  $\rho(r)$ . The positions of the spline knots and the values at the knots are given. Also the first derivatives at the first and last knots are given.

---

$r$ [Å]	$\rho(r)$	$\rho'(r)$ [1/Å]
0.0000	0.000	0.0000
1.8000	$6.3820 \times 10^{-1}$	
1.9000	$7.6541 \times 10^{-1}$	
2.0211	$8.6567 \times 10^{-1}$	
2.2737	$9.2521 \times 10^{-1}$	
2.5264	$8.6200 \times 10^{-1}$	
2.7790	$7.6273 \times 10^{-1}$	
3.0317	$6.0648 \times 10^{-1}$	
3.2843	$4.6603 \times 10^{-1}$	
3.5370	$3.3874 \times 10^{-1}$	
3.7896	$2.3257 \times 10^{-1}$	
4.0422	$1.0905 \times 10^{-1}$	
4.2949	$5.2491 \times 10^{-2}$	
4.5475	$3.9170 \times 10^{-2}$	
4.8001	$3.0828 \times 10^{-2}$	
5.0528	$2.5021 \times 10^{-2}$	
5.3054	$1.4722 \times 10^{-2}$	
5.5600	0.0000	$2.1298 \times 10^{-6}$

TABLE II. Parameters entering the potential energy function from Eq.(4)

Parameter	
$R_0$ [Å]	5.46
$D_0$ [Å]	0.10
$R_\Phi$ [Å]	2.00
$D_\Phi$ [Å]	0.25
A [eV]	7255.44
$\lambda$ [1/Å]	4.42085
B [eV]	1.04897

TABLE III. Parameters used to define the embedding function  $F(\rho)$ . The positions of the spline knots and the values at the knots are given. Also the first derivatives at the first and last knots are given.

$\rho$	$F(\rho)$ [eV]	$u'(\rho)$ [1/eV]
0.0	0.0000	-12.375
0.1	-0.8139	
0.2	-1.2697	
0.3	-1.6799	
0.4	-2.0296	
0.5	-2.2520	
0.6	-2.4272	
0.7	-2.5517	
0.8	-2.6052	
0.9	-2.6440	
1.0	-2.6571	
1.1	-2.6456	
1.2	-2.6087	
1.4	-2.4525	1.0620

TABLE IV. Parameters used to define the pair potential  $\phi(r)$ . The positions of the spline knots and the values at the knots are given. Also the first derivatives at the first and last knots are given.

$r$ [Å]	$\phi(r)$ [eV]	$\phi'(r)$ [eV/Å]
2.0211	1.9601	-7.0273
2.2737	$6.8272 \times 10^{-1}$	
2.5263	$1.4737 \times 10^{-1}$	
2.7790	$-1.8818 \times 10^{-2}$	
3.0317	$-5.7601 \times 10^{-2}$	
3.2843	$-5.1984 \times 10^{-2}$	
3.5369	$-3.7635 \times 10^{-2}$	
3.7896	$-3.7373 \times 10^{-2}$	
4.0422	$-5.3135 \times 10^{-2}$	
4.2949	$-6.3286 \times 10^{-2}$	
4.5475	$-5.4810 \times 10^{-2}$	
4.8001	$-3.7288 \times 10^{-2}$	
5.0528	$-1.8887 \times 10^{-2}$	
5.3054	$-5.8523 \times 10^{-3}$	
5.5600	0.0000	$5.9065 \times 10^{-6}$

TABLE V. Comparison of selected hopping and exchange diffusion barriers on low-index Al surfaces obtained with the present model and in *ab initio* calculations. Al (111) is also included for completeness.

	This work	<i>ab initio</i>
Al (111) hopping	0.04	0.04 <sup>a</sup>
Al (100) hopping	0.60	0.68 <sup>a</sup> , 0.65 <sup>b</sup>
Al (100) exchange	0.50	0.35 <sup>a</sup>
Al (110) $\perp$ hopping	1.13	1.06 <sup>a</sup>
Al (110) $\parallel$ hopping	0.30	0.60 <sup>a</sup>

<sup>a</sup>Reference 15; <sup>b</sup>Reference 28

TABLE VI. Surface formation energies for low index Al surfaces calculated with the present model and with other theories.

System	This work		LDA <sup>a</sup>	
	(eV/atom)	(eV/Å <sup>2</sup> )	(eV/atom)	(eV/Å <sup>2</sup> )
Al(111)	0.38	0.054	0.48	0.070
Al(100)	0.48	0.059	0.56	0.071
Al(110)	0.74	0.065	0.89	0.080

<sup>a</sup>Reference 17

TABLE VII. Step formation energies for low index Al surfaces calculated with the present model and with other theories.

System	This work		LDA <sup>a</sup>	
	(eV/Å)	(eV/atom)	(eV/Å)	(eV/atom)
Al[9(100) $\times$ (111)]	0.055	0.142		
Al[9(100) $\times$ (110)]	0.066	0.240		
Al[9(111) $\times$ (111)]	0.083	0.215	0.082	0.232
Al[9(111) $\times$ (100)]	0.085	0.222	0.088	0.248

<sup>a</sup>Reference 16

